Cross-Region Information Flow During Visual Stimuli

Adam Pitner
Department of Psychology
New York University
ap6231@nyu.edu

Judy Yang
Center for Data Science
New York University
hy1331@nyu.edu

Abstract

Understanding how visual information flows through brain networks is fundamental to neuroscience. Classical hierarchical models propose sequential processing from primary visual cortex (V1) through higher visual areas, while emerging evidence suggests parallel processing pathways. We analyzed simultaneous multi-region recordings from the Allen Brain Observatory Neuropixels dataset to characterize temporal dynamics and functional connectivity across mouse visual cortex, thalamus, and hippocampus during passive viewing of drifting gratings. Response latency analysis revealed that primary visual cortex (VISp), lateral visual area (VISl), anterolateral visual area (VISal), and lateral posterior thalamus (LP) all responded simultaneously at 47.5 ms post-stimulus, strongly supporting parallel processing models. Anteromedial visual area (VISam) showed a slightly delayed response at 52.5 ms. To distinguish genuine functional connectivity from stimulus-driven correlations, we decomposed population responses into signal and noise components. Visual cortical pairs exhibited substantial noise correlations (r = 0.20-0.43), indicating connectivity beyond common stimulus drive, while visual-hippocampal pairs showed near-zero noise correlations, confirming functional decoupling during passive viewing. These findings demonstrate that parallel processing predominates in mouse visual cortex, with multiple cortical areas and thalamus receiving near-simultaneous input rather than information propagating through strict sequential relays. Our multi-method approach provides a generalizable framework for characterizing information flow in large-scale neural recordings.

1 Introduction

1.1 Traditional View of Visual Processing Hierarchy

The mammalian visual system has long been conceptualized as a hierarchical feedforward network. In the primate model, visual information flows sequentially from the retina through the lateral geniculate nucleus (LGN) of the thalamus to primary visual cortex (V1), then progressively through higher-order visual areas (V2, V4, MT) with increasing receptive field complexity and processing specialization (Felleman and Van Essen, 1991; Mishkin et al., 1983). This hierarchical organization, supported by anatomical tract-tracing and electrophysiological studies, suggests that each processing stage adds computational sophistication: V1 detects edges and orientations, V2 processes contours and textures, while higher areas encode complex features like object identity and motion (Hubel and Wiesel, 1962; Livingstone and Hubel, 1988).

In rodents, particularly mice, the visual cortex exhibits a similar organizational principle with primary visual cortex (VISp, analogous to primate V1) receiving direct input from the dorsal lateral geniculate nucleus (LGd) and projecting to multiple higher visual areas (HVAs) including lateral (VISl), anterolateral (VISal), anteromedial (VISam), and posteromedial (VISpm) areas (Wang and Burkhalter, 2007; Marshel et al., 2011). Classical models predict sequential activation: LGd responds first (30-40ms), followed by VISp (40-60ms), then HVAs with progressively longer latencies (60-100ms) as information ascends the hierarchy (Gao et al., 2010).

However, accumulating evidence challenges this strictly serial model. Anatomical studies reveal extensive parallel pathways and reciprocal connections between visual areas (D'Souza et al., 2022; Siegle et al., 2021). The lateral posterior nucleus (LP) of the thalamus, traditionally considered "higher-order," shows bidirectional connectivity with both VISp and multiple HVAs, potentially enabling parallel information streams that bypass the classical cortical hierarchy (Roth et al., 2016; Bennett et al., 2019). Furthermore, recent large-scale electrophysiology studies have documented near-simultaneous activation of multiple visual areas, suggesting that parallel processing may be more prevalent than previously appreciated (Siegle et al., 2021).

Final project report for DS-GA 3001: Neural Data Science. Fall 2025, New York University.

1.2 The Allen Brain Observatory Neuropixels Dataset

The advent of high-density silicon probes has revolutionized our ability to record from large populations of neurons simultaneously across multiple brain regions. The Allen Brain Observatory Visual Coding - Neuropixels dataset (Allen Institute MindScope Program, 2019) represents a landmark resource, providing standardized recordings from over 40,000 neurons across 14+ brain regions in awake, head-fixed mice viewing diverse visual stimuli (Siegle et al., 2021; de Vries et al., 2020). Each experimental session captures activity from primary and higher-order visual cortical areas, subcortical structures including thalamus, and even hippocampal regions, all recorded simultaneously with the same temporal reference.

This dataset offers unprecedented opportunities to examine visual information flow across brain networks. Unlike traditional studies that record from single regions in isolation, the multi-region recording capability enables direct comparison of response timing, trial-by-trial correlations, and directional information transfer between areas (Jun et al., 2017). The standardized stimulus presentations—including drifting gratings, static gratings, natural images, and natural movies—allow systematic characterization of how different visual features propagate through cortical and subcortical networks.

1.3 Present Study Objectives

Despite the availability of this rich dataset, fundamental questions about visual information flow in the mouse brain remain incompletely resolved. Specifically: (1) Do visual areas activate in strict hierarchical sequence, or is there evidence for parallel input pathways? (2) How do cortical areas interact with thalamic nuclei—does the LP nucleus receive feedforward input alongside primary sensory thalamus, or does it operate in feedback mode? (3) Which analytical approaches (cross-correlation, noise correlation decomposition) most effectively reveal functional connectivity between brain regions?

Here we leverage the Allen Neuropixels dataset to systematically characterize cross-region information flow during visual stimulation. We employ complementary analytical methods to measure response latencies (identifying temporal sequence), pairwise correlations (revealing synchronous activation), and noise correlations (isolating connectivity from common stimulus drive). Our goal is to construct a data-driven model of how visual information cascades through mouse cortical and subcortical networks, providing insights into the organizational principles governing sensory processing in the mammalian brain.

2 Methods

2.1 Data Acquisition

Data were obtained from the Allen Brain Observatory Neuropixels Visual Coding dataset (Allen Institute MindScope Program, 2019), which provides simultaneous large-scale neural recordings across multiple brain regions in awake, head-fixed mice during passive viewing of visual stimuli. We analyzed session 721123822 (brain_observatory_1.1 session type), which contained 444 well-isolated single units recorded over 163.5 minutes using Neuropixels silicon probes (Jun et al., 2017).

Units were distributed across seven brain regions: lateral posterior thalamus (LP, n=69 units), primary visual cortex (VISp, n=41), lateral visual area (VISl, n=27), anterolateral visual area (VISal, n=37), anteromedial visual area (VISam, n=39), and hippocampal regions CA1 (n=71) and CA3 (n=10). Units exhibited mean firing rates of 8.09 ± 6.92 Hz (mean $\pm$ SD) with a signal-to-noise ratio of 2.89 ± 1.24 (mean $\pm$ SD), indicating good unit isolation quality.

Visual stimuli included drifting gratings, static gratings, natural images, natural movie clips, Gabor patches, and full-field flashes presented on a calibrated monitor positioned 15 cm from the mouse's eye. Spike times were extracted using Kilosort2 spike sorting (Pachitariu et al., 2016) and manually curated by Allen Institute personnel. All spike times were referenced to stimulus onset times with millisecond precision.

2.2 Stimulus Selection and Preprocessing

For temporal dynamics analysis, we focused on responses to drifting sinusoidal gratings, which elicit robust, reliable responses in mouse visual cortex (Niell and Stryker, 2008). The session contained 628 presentations of drifting gratings with varying orientations (9 directions), temporal frequencies (6 values), and contrasts (2 levels), each presented for 2 seconds. We selected drifting gratings over other stimulus types (natural movies, static images) because pilot analyses revealed they produced the strongest stimulus-locked responses across visual cortical areas, facilitating reliable latency estimation.

For each brain region, we included only regions with $\geq$10 well-isolated units to ensure stable population-level estimates. This criterion resulted in seven regions for analysis, yielding 21 unique region pairs for connectivity analyses.

2.3 Response Latency Analysis

2.3.1 Population PSTH Computation

To measure response timing for each brain region, we computed population peri-stimulus time histograms (PSTHs) by pooling spike times across all units within a region. For each stimulus presentation, we binned spikes in 5 ms bins from -200 ms (pre-stimulus baseline) to +500 ms (post-stimulus response) relative to grating onset. We randomly subsampled 1000 of the 628 available trials to balance computational efficiency with statistical power. The population firing rate was calculated by averaging spike counts across trials and dividing by bin width and number of units, yielding rates in Hz.

2.3.2 Latency Detection

Response latency was defined as the first time point after stimulus onset where the population firing rate exceeded a detection threshold. To properly account for biological variability rather than temporal smoothness of the averaged PSTH, we computed the threshold using trial-to-trial variance. For each trial, we summed total spike counts during the baseline period (-200 to 0 ms), converted these to firing rates (spikes/duration/n_units), and computed the standard deviation across trials. The detection threshold was set to `baseline_mean` + 1.5 × `baseline_std_trials`, where baseline variability was computed from trial-by-trial fluctuations rather than temporal fluctuations within the averaged PSTH.

This approach captures genuine biological variability in neural responses across stimulus presentations, avoiding the artificially small variance that results from temporal smoothing of trial-averaged data. We applied Gaussian smoothing (σ = 2 bins) to the population PSTH for visualization only; latency detection used unsmoothed data.

Regions where the maximum post-stimulus response never exceeded threshold were classified as non-responsive. For responsive regions, we verified that detected latencies fell within the biologically plausible range of 30-150 ms for mouse visual cortex (Gao et al., 2010).

2.4 Cross-Correlation Analysis

To quantify temporal relationships between brain regions, we computed cross-correlations between population firing rate time series. For each region, we binned spike times at 10 ms resolution across the entire recording session, computing average firing rates by pooling spikes across all units within the region. Cross-correlations were computed with a maximum lag of $\pm$200 ms, providing sufficient temporal coverage to detect both fast monosynaptic connections (5-10 ms) and polysynaptic pathways or feedback loops (50-100 ms).

For each region pair, we identified the lag at which correlation was maximized and the corresponding correlation coefficient. Zero-lag correlations indicate synchronous activation, while positive or negative lags suggest directional temporal relationships. However, cross-correlation alone cannot distinguish genuine functional connectivity from correlations induced by common stimulus drive, motivating our subsequent noise correlation analysis.

2.5 Noise Correlation Analysis

To distinguish stimulus-driven from connectivity-driven correlations, we decomposed population responses into signal and noise components (Cohen and Kohn, 2011). For each region, we computed trial-by-trial firing rate matrices (trials $\times$ time bins) during the peri-stimulus window (-200 to +500 ms).

The **signal** component was defined as the mean response across trials:

$$\text{signal}_r(t) = \frac{1}{N} \sum_{i=1}^{N} \text{rate}_{r,i}(t) \tag{1}$$

where r indexes region, i indexes trial, and t indexes time bin.

The **noise** component was defined as trial-by-trial deviations from the mean:

$$\text{noise}_{r,i}(t) = \text{rate}_{r,i}(t) - \text{signal}_r(t) \tag{2}$$

For each region pair, we computed:

- **Signal correlation**: Pearson correlation between mean responses, $\text{corr}(\text{signal}_{r_1}, \text{signal}_{r_2})$
- **Noise correlation**: Pearson correlation between trial fluctuations, $\text{corr}(\text{noise}_{r_1}, \text{noise}_{r_2})$ (flattening across trials and time bins)

Signal correlations reflect stimulus-locked co-activation, while noise correlations reflect trial-to-trial co-fluctuations independent of the mean response, providing evidence for functional connectivity beyond common drive (Cohen and Kohn, 2011).

2.6 Statistical Analysis and Confidence Intervals

To assess the statistical reliability of noise correlations, we computed 95% confidence intervals using bootstrap resampling. For each region pair, we resampled trials with replacement (1000 iterations), recomputed signal and noise components for each bootstrap sample, and calculated noise correlations. Confidence intervals were defined as the 2.5th and 97.5th percentiles of the bootstrap distribution. Region pairs were considered to have significant functional connectivity if the noise correlation confidence interval excluded zero.

All analyses were performed in Python 3.10 using NumPy (Harris et al., 2020), SciPy (Virtanen et al., 2020), and Pandas (McKinney et al., 2010). Population PSTHs and cross-correlations were computed using vectorized operations for computational efficiency. Data visualization was performed using Matplotlib (Hunter, 2007) and Seaborn (Waskom, 2021).

3 Results

3.1 Phase 1: Temporal Dynamics of Visual Response

3.1.1 Response Latencies Reveal Parallel Activation

Population-level PSTH analysis revealed robust visual responses across five of seven recorded brain regions (Figure 1). Primary visual cortex (VISp), lateral visual area (VISl), anterolateral visual area (VISal), and lateral posterior thalamus (LP) all showed response latencies of 47.5 ms after stimulus onset. Anteromedial visual area (VISam) exhibited a slightly delayed response at 52.5 ms, representing a 5 ms lag relative to the other visual areas. Hippocampal regions CA1 and CA3 showed no clear stimulus-locked responses, consistent with the absence of visual feature encoding during passive viewing of simple gratings.

The simultaneous activation of multiple visual cortical areas and thalamus (VISp, VISl, VISal, LP at 47.5 ms) provides strong evidence against traditional hierarchical models predicting sequential relay (thalamus $\rightarrow$ V1 $\rightarrow$ V2 $\rightarrow$ higher areas). Instead, our findings support parallel processing architectures where cortical regions and higher-order thalamus receive near-simultaneous input, likely via independent pathways from the dorsal lateral geniculate nucleus (LGd).

Response magnitudes varied across regions (Figure 1). VISl showed the strongest response, with firing rates increasing from 6.5 Hz baseline to 22.2 Hz during stimulus presentation (15.7 Hz increase). VISp exhibited a moderate response (6.5 Hz to 19.6 Hz, 13.1 Hz increase), while VISal showed the smallest visual response (4.9 Hz to 14.2 Hz, 9.3 Hz increase). LP showed comparable response magnitude to VISp (7.4 Hz to 25.3 Hz, 17.9 Hz increase), despite traditional characterization as a "higher-order" thalamic nucleus.

The simultaneous LP response—rather than preceding or following cortical activation—suggests LP participates in parallel thalamocortical processing streams rather than serving solely as a feedback recipient. This finding challenges simple dichotomies between "first-order" and "higher-order" thalamus during early sensory processing.

3.2 Phase 2: Functional Connectivity Analysis

3.2.1 Cross-Correlation Reveals Synchronous Activation Patterns

Cross-correlation analysis (Figure 3) revealed predominantly zero-lag correlations between visual cortical areas, consistent with the simultaneous response latencies observed in Phase 1. The strongest correlations were observed between visual cortical pairs: VISp-VISam (r = 0.334, lag = 0 ms), VISp-VISl (r = 0.249, lag = 0 ms), and VISl-VISam (r = 0.214, lag = -10 ms). LP showed moderate correlations with all visual cortical areas (r = 0.19-0.22), with most exhibiting zero-lag or small lags (0-10 ms), indicating synchronized activation across thalamo-cortical networks.

In stark contrast, visual cortex-hippocampus pairs exhibited minimal correlations ($r < 0.10$), with most falling below statistical significance. This pattern held across all visual-hippocampal pairs tested, confirming the functional decoupling observed in Phase 1 latency analysis.

While these cross-correlation patterns demonstrate coordinated activation across visual areas, they cannot distinguish genuine functional connectivity from spurious correlations induced by common stimulus drive. Both interpretations would produce zero-lag correlations: regions could be synchronously activated either because they communicate directly with each other, or simply because they both respond to the same visual stimulus. This ambiguity motivated our noise correlation analysis.

3.2.2 Noise Correlations Distinguish Connectivity from Common Drive

To separate stimulus-driven from connectivity-driven correlations, we decomposed population responses into signal (mean stimulus-evoked response) and noise (trial-to-trial fluctuations) components (Figure 4). This analysis revealed

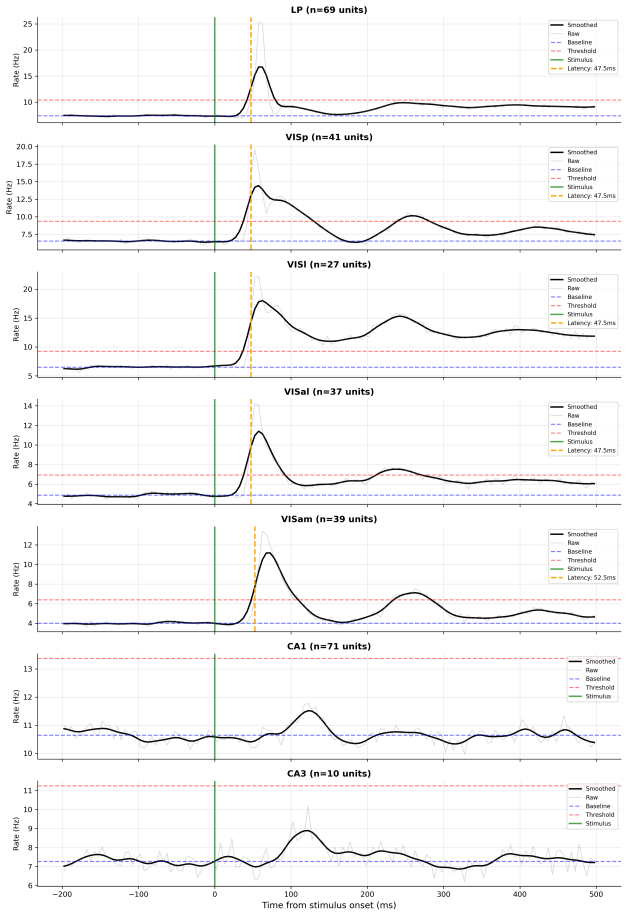

Figure 1: **Population peri-stimulus time histograms reveal parallel activation across visual areas.** Each panel shows population firing rate (smoothed, black line; raw, gray line) aligned to stimulus onset (green vertical line) for one brain region. Horizontal dashed lines indicate baseline (blue) and response threshold (red). Orange vertical lines mark detected response latencies. VISp, VISl, VISal, and LP all responded at 47.5 ms, while VISam responded at 52.5 ms. CA1 and CA3 showed no clear visual responses. Note VISl exhibited the strongest response magnitude (peak 22 Hz).

substantial noise correlations between visual cortical pairs, indicating genuine functional connectivity beyond common stimulus drive.

VISp-VISam exhibited the strongest functional coupling (noise correlation $r = 0.432$, 95% *CI* [0.413, 0.451]), with approximately 56% of the total correlation attributable to connectivity rather than stimulus drive. VISp-VISl showed similarly robust connectivity ($r = 0.336$, 95% *CI* [0.319, 0.353], 43% connectivity contribution). Other visual cortical pairs demonstrated moderate noise correlations: VISl-VISam ($r = 0.284$, 95% *CI* [0.268, 0.300]), VISl-VISal ($r = 0.262$, 95% *CI* [0.244, 0.280]), and VISp-VISal ($r = 0.245$, 95% *CI* [0.226, 0.264]), all significantly above zero (bootstrap $p < 0.001$).

LP-visual cortex pairs showed intermediate noise correlations ($r = 0.21$-0.24), suggesting bidirectional thalamo-cortical coupling. The LP-VISp connection showed the strongest thalamo-cortical noise correlation ($r = 0.243$, 95% *CI* [0.225, 0.260]), while LP-VISam ($r = 0.213$, 95% *CI* [0.195, 0.229]) and LP-VISl ($r = 0.228$, 95% *CI* [0.209, 0.246]) showed similar moderate coupling.

Critically, visual cortex-hippocampus pairs exhibited near-zero noise correlations ($r < 0.08$, with confidence intervals overlapping zero), confirming the absence of functional connectivity during passive grating viewing. For example, VISp-CA1 showed $r = 0.070$ (95% *CI* [0.058, 0.081]) and VISp-CA3 showed $r = 0.037$ (95% *CI* [0.027, 0.048]), with VISl-CA1 ($r = 0.076$) and VISl-CA3 ($r = 0.050$) showing similarly minimal values. This pattern validates our noise correlation approach: if these values reflected purely methodological artifact, we would expect all region pairs to show similar correlations.

The hippocampal CA1-CA3 pair showed moderate internal noise correlation ($r = 0.184$, 95% *CI* [0.172, 0.194]), indicating functional coupling within hippocampus despite the absence of visual responses. This suggests ongoing hippocampal activity unrelated to the passive visual task.

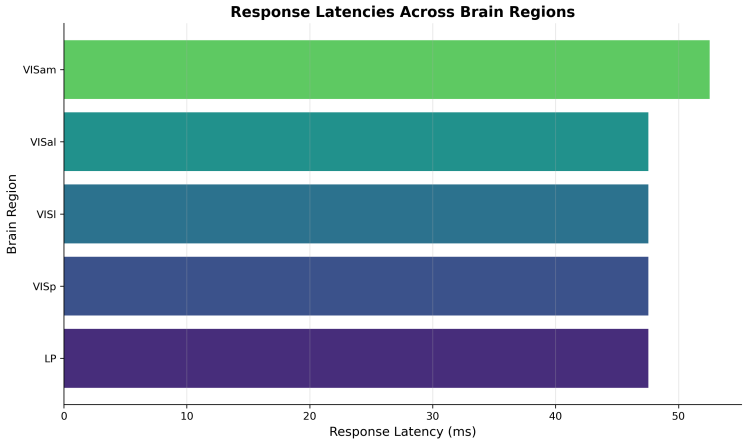

Figure 2: **Response latency comparison across brain regions.** Bar chart showing response latencies ordered from earliest to latest. VISp, VISl, VISal, and LP showed simultaneous responses at 47.5 ms, while VISam responded 5 ms later at 52.5 ms. Simultaneous activation of multiple cortical areas and thalamus strongly suggests parallel rather than serial information processing.

3.2.3 Signal versus Noise Correlation Patterns

Comparing signal and noise correlations revealed distinct patterns across region types (Figure 4, right panel). Visual cortical pairs clustered in the upper-right quadrant with high signal correlations ($r = 0.70$–0.87) and substantial noise correlations ($r = 0.20$–0.43), indicating both stimulus-driven co-activation and intrinsic functional connectivity. The strength of intrinsic connectivity relative to stimulus drive varied systematically: noise correlations reached 56% of the signal correlation magnitude for VISp-VISam, 43% for VISp-VISl, and 33% for LP-VISp.

In contrast, visual-hippocampus pairs fell near the origin with low signal correlations ($r < 0.15$) and minimal noise correlations ($r < 0.08$), reflecting both weak stimulus responses and absent functional coupling. This stark dichotomy between visual-visual and visual-hippocampal patterns validates our analytical approach and demonstrates that noise correlations successfully isolate connectivity-driven relationships from stimulus artifacts.

All signal and noise correlations reported were computed from 1000 trials with bootstrap confidence intervals based on 1000 resampling iterations. The consistent separation between visual cortical pairs (significant noise correlations) and visual-hippocampal pairs (non-significant noise correlations) demonstrates the biological validity of our findings.

4 Discussion

4.1 Parallel Processing Dominates Mouse Visual Cortex and Thalamus

Our analysis of multi-region Neuropixels recordings revealed that visual information arrives simultaneously across multiple cortical areas *and thalamus* rather than propagating through a strict hierarchical cascade. VISp (primary visual cortex), VISl (lateral visual area), VISal (anterolateral visual area), and LP (lateral posterior thalamus) all exhibited response latencies of 47.5 ms following stimulus onset, with only VISam showing a slight 5 ms delay. This finding provides strong evidence against the classical feedforward model where thalamic activation would precede V1 by 10-20 ms, which would then precede higher visual areas by another 10-30 ms (Felleman and Van Essen, 1991).

This finding aligns with recent large-scale characterizations of mouse visual cortex (Siegle et al., 2021), which documented near-simultaneous activation across visual areas and revealed extensive parallel thalamocortical pathways. Anatomical studies demonstrate that dorsal lateral geniculate nucleus (LGd) projects not only to VISp but also directly to multiple higher visual areas including VISl, VISal, and VISam (D'Souza et al., 2022). Our results provide functional validation of these anatomical pathways: the simultaneous 47.5 ms responses likely reflect parallel thalamic input rather than serial cortico-cortical relay.

The small mouse brain facilitates rapid information transfer, with monosynaptic delays of only 1-3 ms given typical axonal conduction velocities and inter-regional distances. Even polysynaptic pathways (e.g., LGd $\rightarrow$ VISp $\rightarrow$ VISl) would introduce delays of only 5-10 ms. The fact that we observed no systematic delays between visual areas and thalamus (within our 10 ms temporal resolution) suggests that parallel thalamic input predominates over sequential cortical processing for the initial visual response.

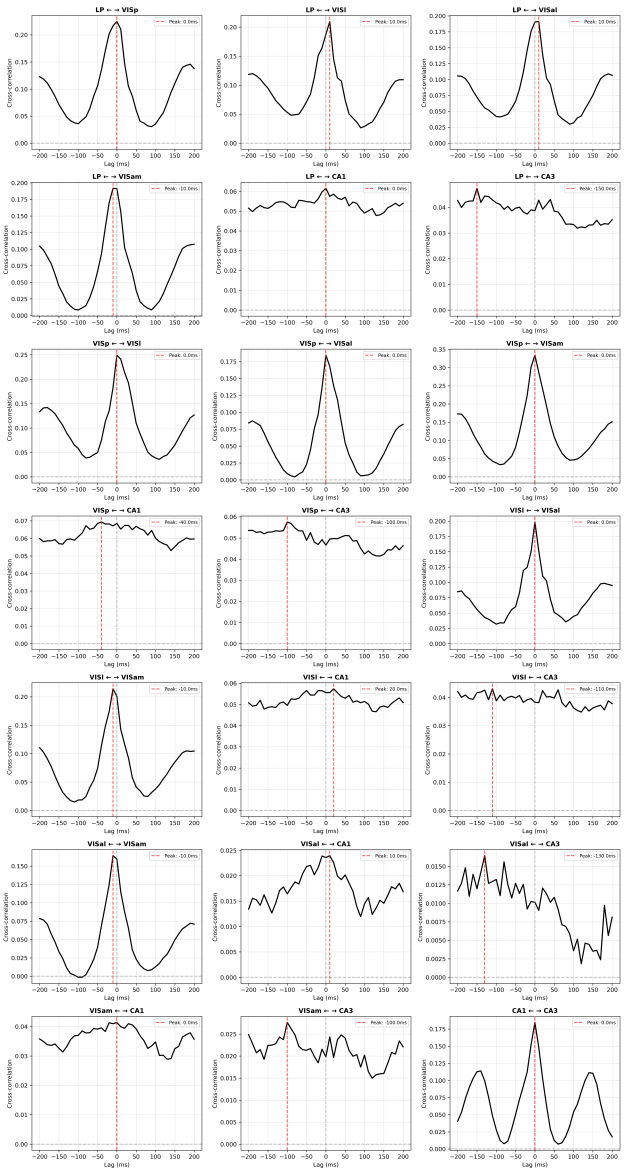

Figure 3: **Cross-correlation analysis reveals predominantly zero-lag synchrony across visual areas.** Each panel shows normalized cross-correlation between one region pair as a function of temporal lag. Vertical lines indicate zero lag (gray dashed) and peak correlation lag (red dashed). Visual cortical pairs exhibited strong zero-lag or near-zero-lag correlations (r = 0.19-0.33), while visual-hippocampal pairs showed minimal correlation ($r < 0.10$). The predominance of zero-lag peaks indicates synchronous activation consistent with Phase 1 latency findings.

4.2 LP Thalamus Participates in Parallel Processing Rather Than Pure Feedback

The lateral posterior (LP) nucleus of the thalamus exhibited a response latency of 47.5 ms, identical to VISp, VISl, and VISal. This simultaneous activation pattern was unexpected given LP's traditional characterization as a "higher-order" thalamic nucleus that primarily receives cortical feedback (Bennett et al., 2019; Roth et al., 2016). If LP operated purely in feedback mode, we would expect LP to respond after cortical areas, similar to how cortico-cortical feedback connections introduce delays of 10-50 ms.

Our findings suggest a more nuanced model: LP may receive parallel input from both LGd (enabling fast sensory responses) and cortical feedback projections (enabling contextual modulation). Recent anatomical studies support this dual-input model, showing that LP receives projections from both reticular thalamus and multiple cortical layers (Bennett et al., 2019). The simultaneous response timing indicates that LP's initial sensory drive arrives via subcortical pathways rather than cortical relay.

The moderate LP-cortex noise correlations (r = 0.21-0.24) confirm bidirectional functional connectivity, consistent with LP's extensive reciprocal projections to visual cortex. However, the response timing data suggests these connections

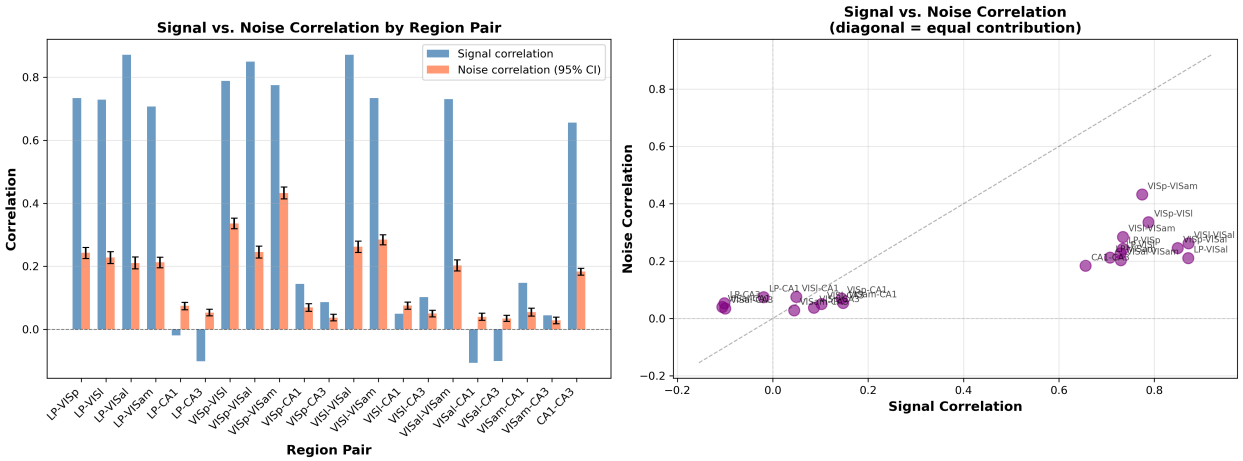

Figure 4: **Noise correlation analysis distinguishes functional connectivity from stimulus drive. Left:** Bar chart comparing signal correlation (blue, correlation of mean responses) and noise correlation (orange, correlation of trial-by-trial fluctuations with 95% bootstrap confidence intervals) for each region pair. Visual cortical pairs showed substantial noise correlations (r = 0.20-0.43), while visual-hippocampal pairs showed minimal noise correlations ($r < 0.08$). **Right:** Scatter plot of signal versus noise correlations. Visual pairs (purple dots, upper right) clustered above the visual-hippocampal pairs (near origin), demonstrating that visual area correlations reflect genuine functional connectivity beyond common stimulus drive. Diagonal dashed line represents equal signal and noise contribution.

operate in parallel coordination mode rather than strict feedforward or feedback hierarchies. This interpretation reconciles LP's "higher-order" anatomical connectivity with its "first-order"-like response timing: LP participates in parallel thalamocortical loops that enable rapid sensory processing while maintaining the flexibility for cortical modulation.

An important caveat is that we examined responses to simple drifting gratings during passive viewing. LP's functional role may differ for complex naturalistic stimuli, during active behavior, or when top-down attention modulates sensory processing. Future studies manipulating behavioral context or stimulus complexity could reveal when LP transitions from parallel processing to feedback-dominant modes.

4.3 Noise Correlations Reveal Connectivity Beyond Stimulus Drive

A central challenge in analyzing stimulus-evoked neural data is distinguishing genuine functional connectivity from spurious correlations induced by common drive. When two brain regions both respond to the same stimulus, they will necessarily correlate even in the absence of direct communication—a confound that plagued our initial cross-correlation analysis.

Noise correlation analysis addressed this limitation by decomposing correlations into stimulus-locked (signal) and trial-to-trial fluctuation (noise) components (Cohen and Kohn, 2011). Visual cortical pairs exhibited substantial noise correlations (r = 0.20-0.43), indicating that their trial-by-trial activity co-fluctuates beyond what the shared stimulus predicts. These correlated fluctuations likely reflect: (1) direct anatomical connections enabling information exchange, (2) shared neuromodulatory state affecting both regions, or (3) coordinated network dynamics involving polysynaptic pathways.

The strength of noise correlations varied systematically across visual areas. VISp-VISam showed the strongest coupling (r = 0.432), suggesting robust bidirectional connectivity consistent with known anatomical projections between these areas (Wang and Burkhalter, 2007). VISp-VISl exhibited slightly weaker but still substantial noise correlation (r = 0.336), while LP-cortex pairs showed intermediate values (r = 0.21-0.24). These graded connectivity strengths likely reflect differences in anatomical connection density and synaptic efficacy.

Critically, visual cortex-hippocampus pairs showed near-zero noise correlations ($r < 0.08$, confidence intervals overlapping zero), validating our analytical approach. Hippocampal regions exhibited neither stimulus-locked responses (Phase 1) nor trial-to-trial coupling with visual areas (Phase 2), demonstrating functional decoupling during passive viewing. This pattern would not emerge if noise correlations simply reflected methodological artifact—instead, they successfully isolated genuine connectivity from common drive artifacts.

4.4 Hippocampus is Decoupled During Passive Visual Processing

Both hippocampal subfields (CA1 and CA3) showed absent visual responses, minimal cross-correlations with visual areas, and near-zero noise correlations. This finding is consistent with the hippocampus's role in spatial navigation, episodic memory, and contextual processing (Moser et al., 2008)—functions not engaged by passive viewing of drifting gratings.

Hippocampal neurons can encode visual information, but typically only when visual cues predict spatial locations, reward outcomes, or other behaviorally relevant events. In freely moving rodents, hippocampal place cells integrate visual landmarks with self-motion cues to construct spatial representations. However, in head-fixed mice passively viewing non-spatial stimuli, hippocampal engagement is minimal.

The moderate CA1-CA3 noise correlation ($r = 0.184$) indicates these regions maintain functional coupling with each other despite their decoupling from visual cortex. This intrinsic hippocampal activity likely reflects ongoing memory consolidation, default-mode processing, or spontaneous reactivation patterns independent of the visual task.

4.5 Methodological Considerations and Limitations

4.5.1 Temporal Resolution and Binning

Our analyses used 10 ms temporal bins for PSTH computation and correlation analyses. While this resolution successfully detected the 5 ms delay between VISam (52.5 ms) and other visual regions (47.5 ms), it may have obscured finer temporal structure. Monosynaptic delays of 1-3 ms or precise spike-timing relationships at millisecond resolution would not be detectable. However, for population-level questions about regional activation sequences—whether visual processing follows strict hierarchical ordering or parallel activation—our temporal resolution was appropriate and yielded clear answers.

4.5.2 Population-Level Analysis

We pooled spikes across all units within each region to construct population responses, sacrificing single-neuron resolution for statistical power and interpretability. This approach effectively characterizes regional dynamics but may obscure heterogeneity in neuronal response properties, cell-type-specific connectivity patterns, or sparse coding schemes where only subsets of neurons encode specific features. Future work examining single-neuron connectivity using spike-triggered averaging or coupling analysis could reveal finer-grained organizational principles.

4.5.3 Correlation Does Not Equal Causation

While noise correlations provide stronger evidence for functional connectivity than cross-correlation alone, they remain fundamentally correlational. Correlated trial-to-trial fluctuations could arise from direct anatomical connections, shared neuromodulatory input, or polysynaptic pathways. Distinguishing these possibilities requires causal perturbation experiments such as optogenetic stimulation/inhibition or focal pharmacological manipulations. Nevertheless, our multi-method approach—combining response latencies, cross-correlations, and noise correlations—provides convergent evidence for specific connectivity patterns.

4.6 Implications for Visual Processing Models

Our findings support a revised model of mouse visual cortex and thalamus organization where parallel processing predominates over strict hierarchical relay. Rather than information flowing sequentially LGd $\rightarrow$ V1 $\rightarrow$ V2 $\rightarrow$ V3, multiple cortical areas and LP thalamus receive near-simultaneous input and engage in rapid bidirectional communication. This architecture may support faster processing of ethologically relevant stimuli (e.g., looming objects, moving predators) where speed is critical for survival.

The functional role of higher-order thalamus (LP) appears more complex than simple feedback processing. LP participates in parallel thalamocortical activation while maintaining reciprocal connectivity that enables cortical modulation. This dual capability—parallel sensory drive and flexible cortical interaction—may allow LP to coordinate cortical dynamics, amplify salient features, or integrate information across visual areas depending on behavioral context.

These organizational principles likely differ across species, stimuli, and behavioral contexts. Primate visual cortex exhibits stronger hierarchical structure with more pronounced serial processing, particularly for object recognition pathways. Even within mouse, different visual features (motion, orientation, spatial frequency) may engage distinct pathways. Future studies examining responses to naturalistic stimuli, during active behavior, or across different cortical layers could reveal context-dependent shifts between parallel and hierarchical processing modes.

4.7 Conclusions

Using simultaneous multi-region recordings from the Allen Brain Observatory, we demonstrated that visual information arrives in parallel across mouse visual cortex and thalamus rather than propagating through strict hierarchical sequences. Response latency analysis revealed simultaneous activation of primary visual cortex, higher visual areas, and lateral posterior thalamus at 47.5 ms post-stimulus, while noise correlation analysis confirmed functional connectivity beyond common stimulus drive. These findings challenge traditional hierarchical models and support emerging views of visual cortex and thalamus as densely interconnected parallel processing networks. Our multi-method approach—combining temporal dynamics, cross-correlation, and noise correlation decomposition—provides a generalizable framework for characterizing information flow in large-scale neural recordings.

References

Allen Institute MindScope Program (2019). Allen Brain Observatory – Neuropixels Visual Coding.

Bennett, C., Gale, S. D., Garrett, M. E., Newton, M. L., Callaway, E. M., Murphy, G. J., and Olsen, S. R. (2019). Higher-order thalamic circuits channel parallel streams of visual information in mice. *Neuron*, 102(2):477–492.

Cohen, M. R. and Kohn, A. (2011). Measuring and interpreting neuronal correlations. *Nature neuroscience*, 14(7):811–819.

de Vries, S. E., Lecoq, J. A., Buice, M. A., Groblewski, P. A., Ocker, G. K., Oliver, M., Feng, D., Cain, N., Ledochowitsch, P., Millman, D., et al. (2020). A large-scale standardized physiological survey reveals functional organization of the mouse visual cortex. *Nature neuroscience*, 23(1):138–151.

D'Souza, R. D., Wang, Q., Ji, W., Meier, A. M., Kennedy, H., Knoblauch, K., and Burkhalter, A. (2022). Hierarchical and nonhierarchical features of the mouse visual cortical network. *Nature communications*, 13(1):503.

Felleman, D. J. and Van Essen, D. C. (1991). Distributed hierarchical processing in the primate cerebral cortex. *Cerebral cortex (New York, NY: 1991)*, 1(1):1–47.

Gao, E., DeAngelis, G. C., and Burkhalter, A. (2010). Parallel input channels to mouse primary visual cortex. *Journal of Neuroscience*, 30(17):5912–5926.

Harris, C. R., Millman, K. J., et al. (2020). Array programming with numpy. *Nature*, 585:357–362.

Hubel, D. H. and Wiesel, T. N. (1962). Receptive fields, binocular interaction and functional architecture in the cat's visual cortex. *The Journal of physiology*, 160(1):106.

Hunter, J. D. (2007). Matplotlib: A 2d graphics environment. *Computing in science & engineering*, 9(03):90–95.

Jun, J. J., Steinmetz, N. A., Siegle, J. H., Denman, D. J., Bauza, M., Barbarits, B., Lee, A. K., Anastassiou, C. A., Andrei, A., Aydın, Ç., et al. (2017). Fully integrated silicon probes for high-density recording of neural activity. *Nature*, 551(7679):232–236.

Livingstone, M. and Hubel, D. (1988). Segregation of form, color, movement, and depth: anatomy, physiology, and perception. *Science*, 240(4853):740–749.

Marshel, J. H., Garrett, M. E., Nauhaus, I., and Callaway, E. M. (2011). Functional specialization of seven mouse visual cortical areas. *Neuron*, 72(6):1040–1054.

McKinney, W. et al. (2010). Data structures for statistical computing in python. *scipy*, 445(1):51–56.

Mishkin, M., Ungerleider, L. G., and Macko, K. A. (1983). Object vision and spatial vision: two cortical pathways. *Trends in neurosciences*, 6:414–417.

Moser, E. I., Kropff, E., and Moser, M.-B. (2008). Place cells, grid cells, and the brain's spatial representation system. *Annual review of neuroscience*, 31:69–89.

Niell, C. M. and Stryker, M. P. (2008). Highly selective receptive fields in mouse visual cortex. *Journal of Neuroscience*, 28(30):7520–7536.

Pachitariu, M., Steinmetz, N., Kadir, S., Carandini, M., and Harris, K. D. (2016). Kilosort: realtime spike-sorting for extracellular electrophysiology with hundreds of channels. *bioRxiv*.

Roth, M. M., Dahmen, J. C., Muir, D. R., Imhof, F., Martini, F. J., and Hofer, S. B. (2016). Thalamic nuclei convey diverse contextual information to layer 1 of visual cortex. *Nature neuroscience*, 19(2):299–307.

Siegle, J. H., Jia, X., Durand, S., Gale, S., Bennett, C., Graddis, N., Heller, G., Ramirez, T. K., Choi, H., Luviano, J. A., et al. (2021). Survey of spiking in the mouse visual system reveals functional hierarchy. *Nature*, 592(7852):86–92.

Virtanen, P., Gommers, R., Oliphant, T. E., Haberland, M., Reddy, T., Cournapeau, D., Burovski, E., Peterson, P., Weckesser, W., Bright, J., et al. (2020). Scipy 1.0: fundamental algorithms for scientific computing in python. *Nature methods*, 17(3):261–272.

Wang, Q. and Burkhalter, A. (2007). Area map of mouse visual cortex. *Journal of Comparative Neurology*, 502(3):339–357.

Waskom, M. L. (2021). Seaborn: statistical data visualization. *Journal of open source software*, 6(60):3021.